Journal of Materials Chemistry C

PAPER

View Article Online
View Journal | View Issue

Cite this: J. Mater. Chem. C, 2017, 5, 12635

MEMS analogous micro-patterning of thermotropic nematic liquid crystalline elastomer films using a fluorinated photoresist and a hard mask process†

David Ditter,[a] Wei-Liang Chen,[b] Andreas Best,[c] Hans Zappe,[d] Kaloian Koynov,[c] Christopher K. Ober *[b] and Rudolf Zentel *[a]

Received 30th August 2017,
Accepted 24th November 2017

DOI: 10.1039/c7tc03958a

rsc.li/materials-c

In this work, we present a method to pattern liquid crystal elastomers (LCEs) in the micrometer range without using any mechanical processing steps to prepare micron sized LCE actuators compatible with microelectromechanical system (MEMS) technology. Multi-layer spin-coating processes are developed to synthesise and structure 300–3500 nm thick LCE films. A water soluble sacrificial layer, a photoalignment layer and a LCE formulation, which is polymerised and crosslinked in its liquid crystal phase, are spin-coated successively onto a substrate. A fluorinated photoresist layer is used to structure LCE films with thicknesses up to 700 nm in a photolithographic and etching process. For thicker LCE films a hard mask process, using hydrogen silsesquioxane (HSQ) as hard mask, is used. Film thicknesses and homogeneities are analysed with profilometry. Actuation motions of LCE layers are investigated before and after patterning and LCE patterns are investigated *via* (polarised optical) microscopy (POM), scanning electron microscopy (SEM) and profilometry. A resolution of 1.5–2.0 microns is achieved with the described techniques, which make deformable micron sized LCE actuators of variable shape and director orientation accessible. The presented results demonstrate the potential of LCEs in MEMS devices.

Introduction

Liquid crystal elastomers are composed of liquid crystals, which are embedded in a weakly crosslinked polymeric network. They combine the properties of polymeric elastomers with the self-organization of liquid crystals.[1–4] Mesogens can either be incorporated in the polymeric backbone (main-chain elastomers) or can be attached *via* flexible alkyl spacers (side-chain elastomers).[5,6] In their liquid crystal state mesogens have locally a direction of preferred orientation, which is represented through a dimensionless vector named director.[4,7,8]

Usually, the director field is split into domains on a macroscopic level and thus statistically distributed, so that there is no overall orientation in untreated samples. To maintain an uniform alignment it is necessary to treat the samples during or before building the elastomer network. Finkelmann has introduced a first approach to synthesise LCEs through orientation of mesogens that are incorporated in a weakly crosslinked polymeric network through uniaxial mechanical stretching.[2] Subsequently, complete crosslinking occurs whereby the director pattern is frozen (Finkelmann method). Nowadays liquid crystals are usually aligned with other techniques and crosslinking as well as polymerisation occurs after alignment. Beside of mechanical forces or shear, electrical or magnetical fields, a flow field – as it is used in microfluidic devices – or photoalignment layers can be used.[3,8–15] After elastomer synthesis aligned mesogens work as an anisotropic solvent for the polymer chains and force them from their favoured isotropic coil into an anisotropic stretched or elongated conformation. As a result the coil dimensions parallel and orthogonal to the director are different.[4,7]

Depending on the system, external stimuli like heat, light, humidity, a change of pH value or mechanical forces can cause a phase transition from the liquid crystal to the isotropic state, in which the polymer chains adopt the favoured isotropic coil conformation.[16–19] This results in a contraction of the network parallel to the prior director and an expansion in the other directions while keeping the LCE volume constant.[10] When removing the

[a] Institute of Organic Chemistry, Johannes Gutenberg-University Mainz, 55099 Mainz, Germany. E-mail: zentel@uni-mainz.de
[b] Department of Materials Science and Engineering, Cornell University, Ithaca NY, USA
[c] Max-Planck-Institute for Polymer Research, Ackermannweg 10, 55128 Mainz, Germany
[d] Department of Microsystems Engineering, Albert-Ludwigs-University, 79098 Freiburg, Germany

† Electronic supplementary information (ESI) available. See DOI: 10.1039/c7tc03958a

external stimulus the system returns to its initial state if the system is above the glass transition temperature T_g. These reversible actuation capacities through the anisotropy-to-isotropy change of macromolecular chains make them an unique class of shape memory materials.[3,4]

Most common actuation stimuli are temperature variations and light irradiation. A great advantage of light is that it can be used remote controlled. It has been shown that those light-sensitive materials can be used as light-sensitive polymer coatings and artificial cilia or to perform transport motions.[18,20–22] On the other hand, not all light-sensitive LCE actuators can be triggered by light as single stimulus at room temperature and in some cases heating to elevated temperature is necessary to facilitate the light induced phase transition.[20] While most LCE phase transitions can be caused by temperature variations, light-sensitive LCEs usually require specific chemical moieties like azo groups.[10,23–29]

To achieve an optimal and evenly distributed temperature control, heating elements have been successfully integrated into LCE devices. This allows, for example, the presetting of strain or stroke without hysteresis. Also more complex deformations like the actuation of an artificial human iris became possible. Platinum heating elements have been integrated and showed very good results. Also temperature controlled lens systems were constructed.[30–32]

The preparation of LCEs has been made – so far – mostly in molds or between glass plates, whereby the director was aligned by surface interactions or magnetic fields.[3] In all these processes each final sample had to be separated mechanically and often pieces are cut as desired. This makes it difficult to produce a large amount of LCE devices for commercialisation. A possible way to overcome this problem may be the use of microfluidic devices, which allows the preparation of many – expanding or contracting – LCE particles, subsequentially.[8–10,15] Beside such "usual" actuations, also core shell particles with fluids inside LCE particles that can be used as micropumps and Janus particles that showed actuation of just one part of the particle could be synthesised.[9,33]

On the other side there is the technology for MEMS production, which is adopted from the processing of semiconductors, with which it is therefore compatible.[34–37] It allows the preparation of actuating parts on the surface of a "wafer-like" object through processing steps like: (i) creation of new layers by evaporation or spin-coating, (ii) their lateral structuring with light and masks and (iii) finally by etching or dissolution.

LCEs are a promising alternative in MEMS devices since they have a couple of advantages in comparison to materials that are used to date. They show larger deformations (up to 400% for main-chain and 70% for side-chain elastomers), but smaller forces than piezo materials and they actuate faster than stimuli-responsive hydrogels, because no mass transport is needed.[4,15,28,38–40]

Additionally, they are lightweight, flexible, disposable, easy to process and cheap what make their perspectives for commercial usages great.[22] However, their applications as soft actuators, micro robotics, atomic force microscopes, microgrippers, micropillars, valves in microfluidic devices and usage in biological systems are limited to single devices because integration is usually complex and must be done manually.[4,7,41–44] For the integration in MEMS devices, it is necessary to pattern LCEs locally, but also to control the director pattern to get complex and desired actuation motions for the particular applications. So far, three-dimensionally patterned director structures in LCEs that show complex shape changes (origami) have been prepared, also with help of photoalignment layers.[12,14,17,45,46] Other approaches deal with two step irradiation patterning processes, where parts of LCE films are crosslinked in its liquid crystal phase in a lithographic process while other parts are crosslinked in its isotropic phase in an accordion or checkerboard like structure what leads to a wide range of actuation motions.[3,45] On the other side, the patterning of LCEs is rarely investigated. Patterning through partial polymerisation and crosslinking of LC mixtures in combination with a dichroic photoinitiator through polarisation holography and subsequent dissolution of weakly crosslinked remaining parts has been reported. Results of this work showed that in principle LCEs can be used as photoresists, but the adhesion to used substrates was really poor, so that no accurate patterns could be observed.[47] The patterning of polymethylsiloxane based LCE films was performed by partial photolithographic irradiation of pre-elastomer formulations by UV-light and dissolution of the non-crosslinked parts. Through etching processes a free standing LCE film actuator could be built.[48] However, with this method it was not possible to vary the director of LCE films locally. Additionally, the described processes may cause swelling of LCE parts through the used solvents which can have a negative effect on alignment and thus actuation properties. Attempts of nanopatterning have been made by etching of block copolymers when blocks show sufficient etching contrast. This can be realised through introducing silicon in one polymer block, but optimisation of etching parameters is difficult and could not be realized yet.[49] Additional patterning was done by soft lithography.[50]

The adoption of MEMS processing technology like used for semiconductors for the preparation of LCEs with complex director pattern might allow their integration in electronic devices. In addition, it would allow full freedom in selecting the desired shape of the final actuator and flexibility with regard to the type of deformation, if it gets possible to select the director pattern during the processing steps. So far, the missing compatibility of LCEs with the available MEMS technologies hindered progress in this area.[51] The problems associated with such a process are, however, that it requires a multi-layer setup with organic layers, which might dissolve during the creation of additional layers by spin-coating. This problem seems to be especially severe for liquid crystal materials, where the solvents used to spin-coat and process the photoresist might swell the LC material and destroy its director field. This is probably the reason, why such experiments have not been reported so far.

However, here we want to show that the processing of LCEs in the micrometer range by lithographic processes (that is only by spin-coating, illumination, redissolution or etching) is possible, if photoresists with orthogonal solubility are used.[52–55] Thereby, we

want to bring them a step closer to real life applications in MEMS devices.

Results and discussion

Preconditions and spin-coating process

LCE films should be patterned in a photolithographic and etching procedure with a resolution in the micrometer range. It should also allow a local variation of the order parameter. For this purpose a multi-layer spin-coating process with – at least – four layers has to be developed:

1. A sacrificial layer that enables the removal of the LCE layers or pieces from a substrate to investigate their actuation properties before and after patterning.

2. An optical addressable orientation layer that allows the lateral variation of the director of LCE layers in every desired way.

3. The LCE layer itself.

4. A photoresist that can be spin-coated, developed and stripped under orthogonal conditions. All used solutions must show orthogonal solubility to LCE and sacrificial layer.

To provide orthogonal conditions the sacrificial layer should be soluble only in water. The photoalignment layer should not show any solubility in water or organic solvents. Rolic Technologies Ltd provides such kind of photoresists that are not soluble in water and decrease their solubility in organic solvents through crosslinking during irradiation with light in the UV range. LCE precursor formulation and LCE itself should be soluble and swell just in organic solvents. Photoresist as well as developer and stripper should not affect any other layers. This can be achieved by using fluorinated photoresists that can be processed from fluorinated solvents. Such photoresists were developed for the processing of polymeric semiconductors in the field of organic electronics and consist of highly fluorinated compounds.[53]

The developed three-layer spin-coating process to synthesise LCE layers is shown in Fig. 1.

Silicon or glass wafers were used as substrates. Polyacrylic acid (PAA) neutralised with sodium hydroxide was spin-coated as an aqueous solution as water-soluble sacrificial layer. The sodium salt of PAA is soluble in water and insoluble in organic solvents before and after photolithography and it was previously described to achieve homogeneous layers when spin-coating it from aqueous solutions.[56] This is an alternative to the use of other water soluble sacrificial layers like poly(2-ethyl-2-oxazoline) to obtain free-standing LCE films.[57,58]

Alignment was achieved with the photoalignment layer ROP-108 EXP001® from Rolic Technologies Ltd. The layer is based on cinnemate polymers which are crosslinked through [2+2] cycloaddition through linear UV light irradiation similar to previous reported photoalignment layers from this company.[59] Through *in situ* crosslinking the solubility in organic solvents decreases and the layer becomes thermally and optically stable. No manual rubbing is necessary what might create dust, static electricity or damage the layer. In addition, the director

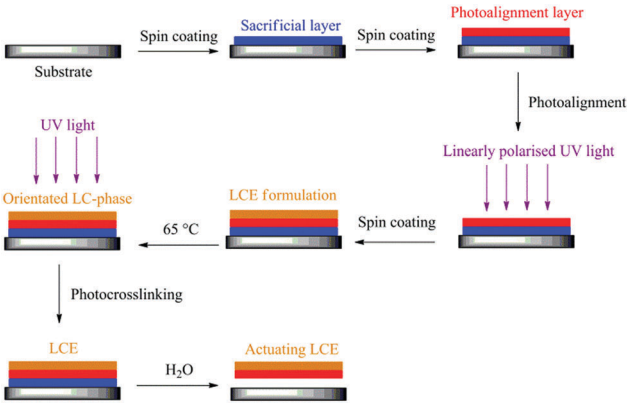

Fig. 1 Schematic drawing of spin-coating process to obtain LCE layers 300 to 3500 nm thick. Sacrificial layer (poly(acrylic acid) neutralised with sodium hydroxide) and photoalignment layer (ROP-108 EXP001®) are spin-coated one after another on a glass or silicon substrate. The photoalignment layer is irradiated with linear polarised UV light to perform crosslinking and predetermine the alignment of LC monomers. A LCE formulation is spin-coated afterwards and heated in its liquid crystal phase. After crosslinking and polymerisation under oxygen-free conditions LCE layer and photoalignment layer – that stick on each other – can be removed in water.

alignment can be varied locally by step wise irradiation with polarised light. LC monomers which are described in the following are aligned parallel to linear polarised UV light since cyclobutane photoderivates align parallel to the polarisation direction, which in turn induces alignment of monomers.

Thirdly, a formulation out of 86 mol% of a liquid crystal monomer (4′-acryloyloxybutyl-2,5-(4′-butyloxybenzoyloxy)-benzoate), 9 mol% of a crosslinker (1,6-hexanediol diacrylate) and 5 mol% of an initiator (diphenyl(2,4,6-trimethylbenzoyl)-phosphine oxide) was spin-coated as solution in tetrahydro-furan. The components are shown in Fig. 2.

The formulation was already used to build particles in microfluidic devices and actuation properties were optimised.[60] Actuations up to 70% were reported.[15] The used LC monomer shows a crystalline to nematic phase transition at 72 °C and a liquid

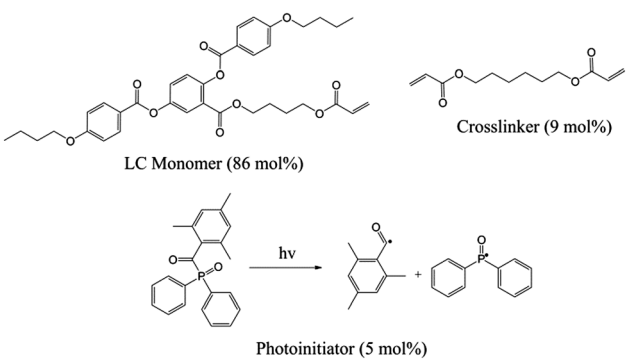

Fig. 2 Chemical structures of spin-coated LCE formulation. The formulation consists out of 86 mol% LC monomer (4′-acryloyloxybutyl-2,5-(4′-butyloxybenzoyloxy)-benzoate), 9 mol% crosslinker (1,6-hexanediol diacrylate) and 5 mol% photoinitiator (diphenyl(2,4,6-trimethylbenzoyl)-phosphine oxide).

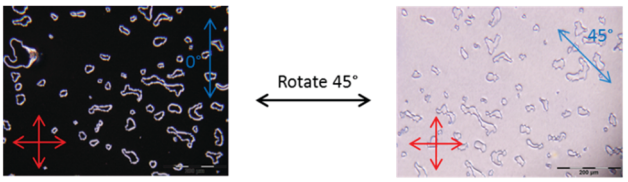

Fig. 3 Optical images of uniaxial aligned LCE layers between crossed polarisers. The red arrows indicate the position of the crossed polarisers and the blue arrows indicate the director's alignment (scale bar: 200 μm).

crystal to isotropic phase transition at 98 °C and was first synthesised in the group of Keller.[39] The polymerised LCEs obtained from the depicted LCE formulation above show an increased clearing temperature at about 120 °C. The glass transition temperature T_g of the LCE is at 40 °C.[39] Thus it will show the properties of an LCE between about 70 °C (30 °C above T_g) and 120 °C. When heating the formulation – on top of the alignment layer – to its liquid crystal phase, alignment can be checked *via* POM. A dark and a bright state can be observed if the director is aligned parallel and at 45° to the crossed polarisers (Fig. 3). Polymerisation and crosslinking of the oriented LC monomers were performed with UV light irradiation under an argon atmosphere since oxygen acts as inhibitor for TPO, radical polymerisation and crosslinking.

Analysis and actuation properties of spin-coated LCE films

Thicknesses and homogeneities of all layers were analysed by profilometry based on white light confocal microscopy. Results are summarised in Table 1. The roughness value R_q represents the average quadratic deviation of the roughness-ordinate values from the centre line (standard deviation of profile ordinates). The waviness value W_t represents the difference between the highest and lowest profile value in a specific evaluation range that is 750 microns in the cases evaluated. All data conform with DIN EN ISO 4287 and DIN EN ISO 4288. Homogeneities of sacrificial layers and photoalignment layers – after spin-coating them on top of the sacrificial layers – showed good results. In relation to total thicknesses R_q values of under 1% and W_t values between 1 and 5% are observed. We tried to keep the thicknesses of photoalignment layers as thin as possible, since they stick to LCE layers after removal from substrates and thus work as resistance for actuations (see Fig. 1, lower line). Homogeneities became worse after spin-coating of LCE layers. R_q values between 1 and 8% and W_t values between 5 and 10% in relation to the total thicknesses were measured.

Table 1 Measured thicknesses and homogeneities after spin-coating of sacrificial layer (PAA), photoalignment layer and LCE layer one after another on a glass substrate. Measurements are based on profilometry. Roughness values (R_q) and waviness values (W_t) conform with DIN EN ISO 4287 and DIN EN ISO 4288

Layer	R_q [nm]	W_t [nm]	Thickness [nm]
Polyacrylic acid	4–6	20–80	1400–1500
Photoalignment layer	4–6	30–70	40–100
LCE layer	20–150	100–400	300–3500

R_q: roughness; W_t: wavyness.

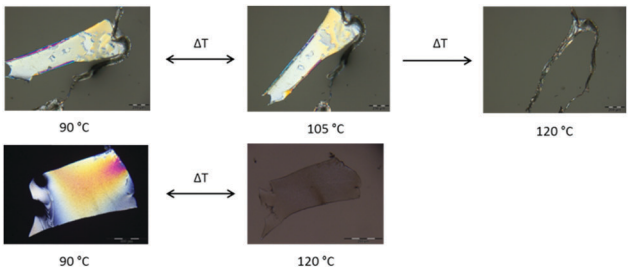

Fig. 4 Microscope images of cut LCE layers between 90 and 120 °C. Upper images: Three dimensional bending motion of a piece of a 1.3 micron thick film. Between 90 °C and 105 °C a reversible actuation can be seen. At 120 °C the ends of the film stick together and as a result do not show a reverse actuation. Lower images: Reversible two-dimensional elongation and shrinkage of a piece of a 3.2 micron thick film (scale bar: 200 μm).

A possible reason might be an incomplete conversion at the surface of the layers because small amounts of oxygen could function as inhibitor for polymerisation and crosslinking reactions. But most important, these LCE layers keep the orientation of the uncrosslinked LC monomer formulation.

To determine the actuation of LCE films above T_g, they were removed from their substrates by dissolution of the sacrificial layer in water and their temperature dependent actuation behaviour was investigated under a microscope – on a silicon oil covered microscope slide – with the help of a heating stage. The silicon oil is necessary to prevent sticking of the LCEs on the microscope slides. LCE films were cut into pieces with a scalpel. It could be shown that actuation properties are thickness dependent. Films, which are thinner than 700 nm did not show any actuation motions through heating above clearing temperature. Films 1.3 to 1.7 microns thick showed three-dimensional twisting and bending motions, while films 3.0 micron and thicker showed a pure two-dimensional shrinkage and elongation with values up to 43% as expected for this type of material. The reason for this thickness dependent behaviour might be the photoalignment layer that sticks to the LCE film and acts as a resistance against deformation. Thin films cannot overcome this resistance while thicker films are able to do so. In Fig. 4 examples of bending as well as shrinkage and elongation are shown. Because actuation is stronger at the LCE side opposite to the photoalignment layer bending occurs at the upper side of films.

Patterning process

Patterning should be done with a suitable photoresist which allows the photolithographic and etching procedure without affecting any other layers. Usage of common photoresists which are dissolved, developed or stripped in organic solvents like methyl isobutyl ketone or 2-methoxy-1-methylethylacetate can cause swelling of the used LCE layers and most other LCE networks. As a result, films can lose their homogeneous LC alignment. One example for this is shown in the ESI† (Fig. SI1). Additionally, sometimes cracking of the films was observed when they got in physical contact with organic solvents which might be a consequence of swelling and deswelling. On the other hand,

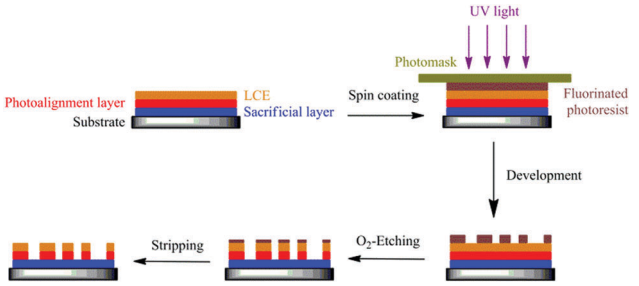

Fig. 5 Schematic drawing of patterning process. A positive fluorinated photoresist is spin-coated on top of the LCE layer which is synthesised as shown in Fig. 1 and irradiated with 365 nm UV light through a photomask. The resist layer is developed in a fluorinated developer and the LCE film is etched in oxygen plasma, subsequently. Remaining resist is stripped off with a fluorinated stripper what results in desired LCE structures of any shapes in dependence of the used photomask.

developing and stripping of resists often takes place in aqueous solutions. Since any aqueous solution dissolves the used sacrificial layers, those photoresists are no alternative as well.

To overcome these problems a special fluorinated photoresist that was developed by Orthoganol Inc. to process polymeric semiconductors was used.[53] Those resists are dissolved, can be developed and stripped in fluorinated solvents and as a result do not swell or dissolve any previously used layers. The patterning process is shown in Fig. 5. After spin-coating, the photoresist is irradiated with 365 nm UV light through a photomask. LCE layers are etched in oxygen plasma after development while all areas covered with the photoresist are protected. After etching, remaining resist is stripped off. With the process shown it is possible to create structures of any desired shapes. An example of patterned stripe like structures is shown in Fig. 6. No loss of alignment is observed which proves the orthogonality of the procedure. In addition, homogeneities do not change after resist spin-coating.

However, the drawback of the process is that there is an etching limit for LCE thickness. This situation is due to the etching rates of photoresist and LCE. While 9.90 nm resist per second is etched under the used etching conditions, just 4.25 nm LCE layer per seconds is etched. This leads to a selectivity of 0.43. The reason for this behaviour is probably due to the benzene groups of the LCE that are more difficult to oxidise than non-aromatic resist polymers.[61–65]

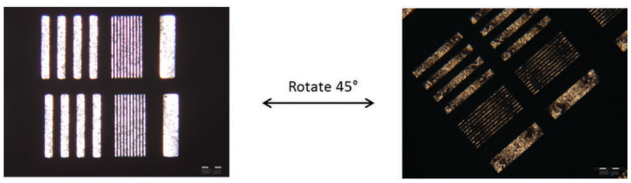

Fig. 6 Microscope images of uniaxial aligned stripe like structured LCE films between two crossed polarisers. On the left image LCE stripes and their director are at a 45° angle to crossed polarisers. On the right image the director of LCE stripes is parallel to one of the crossed polarisers. Dark and bright images proof that there is no loss of alignment after the patterning process (scale bar: 200 μm).

Selectivity in combination with a maximum photoresist thickness of 1.5 microns, which can be achieved through spin-coating, does not allow etching of films thicker than 600–700 nm.

Modification to a hard mask process

To be able to etch thicker films it is necessary to increase the "etch resistance" of the layer protecting the LCE films from oxygen plasma. This can be done by adding a layer of HSQ. This inorganic compound is highly resistant to oxygen plasma since no volatile products can be formed. The hard mask process thus developed consists of the steps shown in Fig. 7. First cyclised transparent optical polymer (CYTOP), an amorphous fluorinated polymer, was spin-coated on top of the LCE as a fourth layer that functions as a second sacrificial layer. Afterwards, a 6 mol% HSQ solution was spin-coated as hard mask. At last the fluorinated photoresist was spin-coated on top, irradiated with 365 nm UV light through a photomask and developed as described before. CYTOP as a fluorinated compound is not affected through fluorinated solvents since it needs some physical forces to remove it due to its bad solubility. Additionally, development was performed through a puddle development whereby developer should not get in contact to CYTOP layer.

HSQ is etched in a plasma mixture out of tetrafluoromethane, trifluoromethane and argon with a rate of 1.7 nm per second. Subsequently, CYTOP as well as LCE and the photoalignment layer below can be etched in oxygen plasma without affecting areas under HSQ. CYTOP etching rate is 7.8 nm per second and photoalignment layer etching rate is 6.6 nm per second. Etching times can be calculated and the endpoint can be checked through POM (loss of LCE birefringence). In the end, HSQ and CYTOP can be removed either through etching or in a CYTOP solvent like hydrofluoroether Novec HFE-7300. When removal of CYTOP takes place in oxygen plasma, etching of PAA layers occurs as well. Otherwise PAA layers are not affected. With the reported procedure it is possible to structure LCE layers of any thickness. Layer thicknesses and homogeneities are investigated by profilometry. Results are shown in Table 2. The layer thickness

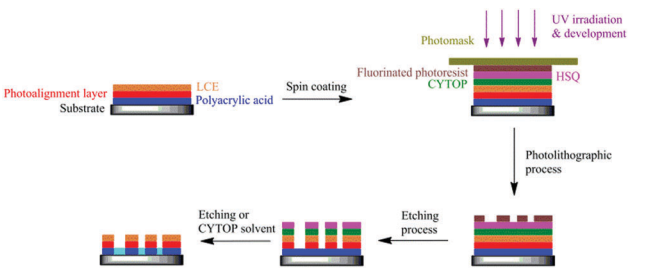

Fig. 7 Schematic drawing of hard mask process. CYTOP, HSQ and fluorinated photoresist are spin-coated on the LCE film, respectively. The fluorinated photoresist is irradiated with 365 nm UV light through a photomask and developed with a fluorinated developer through puddle development. HSQ is etched in a plasma mixture out of CF_4, HCF_3 and argon. CYTOP, LCE and photoalignment layer below are etched in oxygen plasma, subsequently. Remaining CYTOP and HSQ are either removed through etching – what also results in PAA etching – or through dissolution of CYTOP in hydrofluoroether Novec HFE-7300 what does not have any effect on the PAA layer.

Table 2 Measured thicknesses and homogeneities after spin-coating CYTOP, HSQ and fluorinated photoresist one after another on LCE layers. Measurements are based on profilometry. Roughness values (R_q) and waviness values (W_t) conform with DIN EN ISO 4287 and DIN EN ISO 4288

Layer	R_q [nm]	W_t [nm]	Thickness [nm]
CYTOP	40–100	200–400	1000–1200
HSQ	30–100	100–300	150–200
Photoresist	30–100	100–300	1400–1500

R_q: roughness; W_t: wavyness.

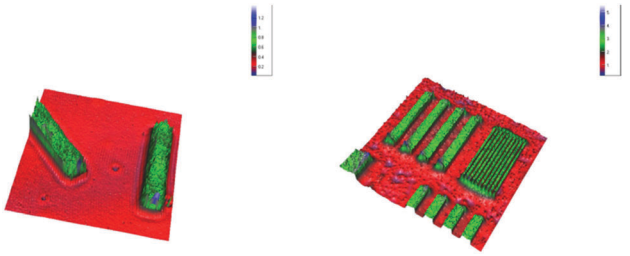

Fig. 8 Three-dimensional profilometry images based on white light confocal microscopy. Left image: 400–500 nm thick LCE stripes patterned with pure photoresist. Right image: About 2.0 micron thick LCE stripes patterned with a hard mask process using HSQ as hard mask. CYTOP and HSQ were removed by dissolution in hydrofluoroether Novec HFE-7300 (colour dependent scale bars in micrometer are shown at the upper right corners of the images – left image: 1.2 μm in 0.2 μm steps; right image: 5.0 μm in 1.0 μm steps).

of CYTOP was made as big as possible because HSQ was spin-coated in an organic solvent that can cause LCE swelling. Since CYTOP is spin-coated in fluorinated solvents it does not affect LCEs and, in the following, works as a protective layer. Similar patterning processes where CYTOP was used as a protective layer and photoresists materials were spin-coated afterwards were reported previously.[66,67] Through dynamical spin-coating and direct drying of the HSQ solution we tried to prevent contact of the organic solvent with the LCE layer. In consequence, no loss of alignment was observed.

Successful hard mask and patterning procedures were proofed with two-dimensional polarised optical microscope images shown in Fig. 6, with which also the alignment can be checked, and with SEM images shown in the ESI† (Fig. SI2). Three-dimensional images could be measured with profilometry based on white light confocal microscopy with which structures as well as structure thicknesses could be confirmed. Two examples of stripe like structures patterned with the pure photoresist and with the hard mask process are shown in Fig. 8. Left image shows 400–500 nm thick LCE stripes made with the pure photoresist. The right image shows about 2.0 micron thick LCE stripes which were made with the hard mask process. In the case shown CYTOP and HSQ were removed through dissolution of CYTOP in hydrofluoroether, so that etching of PAA can be neglected. All described patterning procedures are highly reproducible.

Resolution

Irradiation and development times were optimised for the fluorinated resist used in contact mode with a contact aligner and in projection mode with a projection printing system or "stepper". In contact mode lateral resolution of 3.5–5.0 microns and in projection mode resolution of 1.5–2.0 microns could be achieved. In contact mode a chromium photomask was pressed onto the photoresist layer, which was irradiated through this mask. In projection mode the stepper provided a sophisticated lens system in combination with a precise control over position that results in more accurate patterns. In contrast to contact or proximity mode 2–10 times smaller structures are typically possible in projection mode.[68] Microscope images of LCE layers that were patterned with a resolution mask in projection mode are shown in Fig. 9.

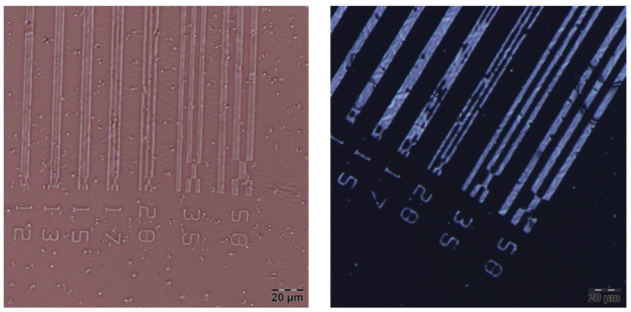

Fig. 9 Microscope images of – with a resolution mask – patterned LCE layers. Photolithography is made in projection mode. Images show resolutions between 1.5 and 2.0 microns. The left image shows a sample investigated with microscopy and the right image shows a sample investigated with POM (scale bars: 20 μm).

Actuations after patterning process

To investigate actuation motions after the patterning processes, stripes with the director parallel to the long axis, the short axis and at a 45° angle to the long (or short) axis were made and detached from the substrate. We expected no actuation for up to 700 nm thick films and bending and twisting motions as well as shrinkage and elongation for thicker films as observed for the unpatterned LCEs (Fig. 4). Again, for LCE films with a thickness up to 700 nm we could not observe any actuations at all. Here obviously the remaining stiff photoalignment layer hinders the movement of the thin LCE film. For thicker films a two-dimensional shrinkage and elongation could be detected. The dominant type of deformation was now, however, bending (see Fig. 10 and 11).

A clear experimental separation of these types of deformation is complicated, as very tiny LCE stripes move around on

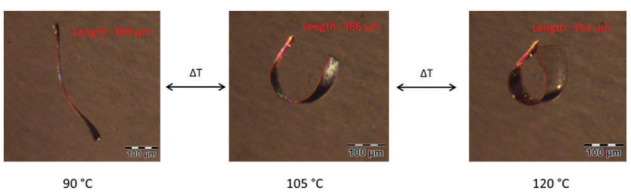

Fig. 10 Microscope images of a lateral 400 × 100 μm LCE stripe between 90 °C (left) and 120 °C (right) that shows an actuation of 13% in this temperature range. The length values (red) are obtained following the red lines shown in the images. The LCE layer from which the stripe originates was processed in a hard mask process using HSQ as hard mask (scale bar: 100 μm).

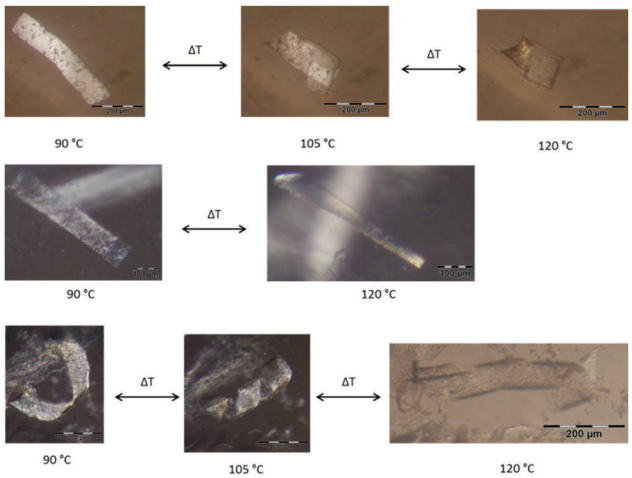

Fig. 11 Microscope images of actuating LCE stripes between 90 and 120 °C after patterning. Upper images: Bending motion of a LCE stripe with its director along the long axis (scale bar: 200 μm). Middle images: Bending motion of a LCE stripe with its director along the short axis (scale bar: 100 μm). Lower images: Twisting motion of a LCE stripe with its director at a 45° angle to the long axis (or short axis) (scale bar: 200 μm).

the oil surface on which the LCE stripes are investigated, change their orientation during actuation and as a result are very difficult to handle. An example of a 400 × 100 micron stripe, which is lying on its side, is presented in Fig. 10. The lengths of the long axis at 90 °C, 105 °C and 120 °C are measured using a microscope imaging software, which shows a clear contraction of 13% (besides some bending). Another sample of a 500 × 100 micron stripe, which shows a contraction of 19%, is shown in the ESI† (Fig. SI3).

Besides this, bending is the dominating deformation and it occurs parallel to the director. Examples are shown in Fig. 11. All deformations are completely reversible and after 20 actuation cycles no differences in actuation properties could be observed. Bending actuation takes about 10 seconds while unbending takes about 20 seconds. Stripes with the director parallel to their long axis role-up to rolls (upper image row), while stripes with the director parallel to the short side role-up to tubes (middle image row). Stripes with the director at a 45° angle to the long (or short) axis role-up to spirals (lower image row). In the case shown below, the helix structure can be clearly seen at 105 °C. At higher temperatures twisting goes on until approximately 120 °C. In this state the windings of the stripe touch each other what makes it difficult to see the resulting helix structure of the transparent (isotropic) material. The stripe also sticks, by accident, at one end to the substrate what links the movement to the substrate. This example demonstrates thus the potential of the used LCE patterning procedure for MEMS devices, where one or both ends of LCE could be attached to different parts of the device. Through temperature induced deformation a reversible movement of one end – relative to the substrate – can be induced. The length change can be used thereby to move the free end relative to the substrate. In many cases the geometry of the object does not allow the LCE to be deformed and thereby suppress bending.[30] On the other side, bending might be interesting to shift an object away from the substrate. One example to embed the LCE in a MEMS device might be an artificial iris. In this case the LCE could be spin-coated on a photoalignment layer that predetermines a radial alignment. After patterning the LCE in an iris like structure, thin film heaters can be integrated and the aperture etched from below. The artificial iris can then be opened or closed through temperature variations. The development of an iris structure from an LCE has been described before.[30,69] However, this structure had always to be integrated afterwards manually into the setup.

The dominating role of bending (compared to the unpatterned films) may be just a consequence of the many processing steps, especially when using the hard mask process, which increase the difference between upper and lower sides of the LCE stripes and make the deformation of both sides less symmetric. As we always observed a bending of the film away from the substrate, the actuation at the upper side of the film should be stronger.

Experimental section

Materials and reagents

Polyacrylic acid 25% (w/v) was purchased from Polysciences (Warrington, PA). 1,6-Hexanediol diacrylate was purchased from Alfa Aesar. Diphenlyl(2,4,6-trimethylbenzoyl)phosphine oxide, sodium hydroxide, 1000 cSt and 10 000 cSt silicon oils and tetrahydrofuran were purchased from Sigma Aldrich. OSCoR 5001 photoresist, Developer 100 and Stripper 903 were purchased from Orthogonal Inc. XR-1541-002 resist (hydrogen silsesquioxane 6 mol% solution) was purchased from Dow Corning. ROP-108 EXP001® was purchased from Rolic Technologies Ltd CYTOP (CTX-809SP2) was purchased from Bellex International Corporation. Hydrofluoroether Novec HFE-7300 was purchased from 3 M. Hellmanex® III concentrate was purchased from VWR. Microscope slides (size: 76 × 26 mm, thickness: 1 mm) were purchased from CARL ROTH. Silicon wafers (diameter: 100 ± 0.5 mm, thickness: 475–575 μm) were purchased from WRS Materials. 4′-Acryloyloxybutyl-2,5-(4′-butyloxybenzoyloxy)benzoate was synthesised as described in the literature.[44]

Spin-coating process and analysis of LCE film actuations

Microscope slides or silicon wafers were cut into 25 × 25 mm pieces and rinsed for 3 minutes with a Hellmanex III solution, deionised water and ethanol – respectively – and dried in a nitrogen stream. Afterwards they were treated in an oxygen plasma oven (model: PlasmaPrep$_5$) from Gala Instrumente GmbH for 5 minutes with a power of 100 W. PAA was set to pH 7–8 with a saturated aqueous sodium hydroxide solution and diluted with deionised water to a 13–14 w% aqueous PAA solution. Substrates were covered with 0.1 ml of this solution and spin-coating occurred at 3000 rounds per minute (rpm) with an acceleration of 3000 rpm per second to final speed for 60 seconds. They were dried at 150 °C for 2 minutes on a hot plate and allowed to cool to room temperature. 40 μl ROP-108 EXP001® photoalignment layer solution was spin-coated dynamically

on top of the PAA layer at 2000 rpm for 60 seconds and dried for 10 minutes at 150 °C on a hot plate. Substrates were allowed to cool to room temperature and the photoalignment layer was irradiated with linear polarised UV light (UV source: Oriel LSH302 (500 W) lamp) with an angle of incidence of 90° using a polariser from OLYMPUS U-POT Japan that pass UV light over 300 nm. In dependence of the desired LCE thickness 40 μl of a solution out of 8–20 mg LC monomer 4′-acryloyloxybutyl-2,5-(4′-butyloxybenzoyloxy)-benzoate (86 mol%) and the according amounts of initiator TPO (5 mol%) and crosslinker 1,6-hexanediol diacrylate (9 mol%) in 100 μl tetrahydrofuran were spin-coated dynamically between 1800 and 4800 rpm. The formulation was brought in its liquid crystal phase at 65 °C and alignment was checked *via* POM (microscope model: Olympus BX51). The formulation was then polymerised and crosslinked under oxygen-free conditions.

To remove LCE layers the samples were placed in water for 10 minutes. Afterwards LCE layers were cut into pieces with a scalpel and placed on a microscope slide covered with 1000 or 10 000 cSt silicon oil. The LCE pieces were heated and cooled with a microscope hot-stage (model: Linkam TMS 94). Actuation behaviour was investigated *via* (polarised optical) microscopy and images were taken using a microscope camera (model: Olympus DP22) and analysed using a microscope imaging software (Olympus cellSens Standard).

Patterning process of up to 700 nm thick films

0.3 ml OSCoR 5001 photoresist was spin-coated on top of the LCE layer at 1000 rpm with an acceleration of 1000 rpm per second to final speed for 60 seconds. Soft bake at 90 °C was performed for 2 minutes on a hot plate. The photoresist was irradiated with 365 nm UV light with an ABM contact aligner or GCA 200 Autostep DSW i-line Wafer Autostepper with a dose range of 60 mJ cm^{-2} through a chromium photomask. A post-exposure bake at 90 °C for 3 minutes and a double puddle development for 80 seconds with developer 100 solution were performed, respectively. In dependence of the film thickness, LCE films were etched in oxygen plasma with a Trion Minilock III plasma etcher from Trion Technology (recipe: pressure: 20.0 mT, inductively coupled plasma-radio frequency (ICP-RF): 300 ± 10 W, reactive-ion etching-radio frequency (RIE-RF): 20 ± 10 W, temperature: 20 °C, standard cubic centimeters per minute (sccm) (oxygen): 25 cm^3 min^{-1}). Remaining OSCoR 5001 photoresist was stripped off with Stripper 903 solution in a double puddle development after 80 seconds, respectively.

Hard mask process for LCE films thicker 700 nm

LCE layers were covered with 0.1 ml CYTOP (CTX-809SP2) and spin-coating occurred at 3000 rpm with an acceleration of 4000 rpm per second to final speed for 2 minutes. Substrates were dried at 110 °C for 5 minutes and heated to 185 °C with a rate of 5 °C per minute on a hot plate. After 10 minutes substrates were allowed to cool to room temperature and treated for 30 seconds with oxygen plasma to create a hydrophilic surface for subsequent material deposition. 50 μl HSQ solution was spin-coated dynamically on top of CYTOP (CTX-809SP2) at 1000 rpm for 60 seconds and dried for 5 minutes at 150 °C on a hot plate. Substrates were allowed to cool to room temperature. OSCoR 5001 photoresist was spin-coated on HSQ at 1000 rpm with an acceleration of 1000 rpm per second to final speed for 60 seconds. Soft bake at 90 °C was performed for 2 minutes on a hot plate. The photoresist was irradiated with 365 nm UV light with an ABM contact aligner or GCA 200 Autostep DSW i-line Wafer Autostepper with a dose range of 60 mJ cm^{-2}. A post-exposure bake at 90 °C for 3 minutes and afterwards a double puddle development for 80 seconds with Developer 100 solution were performed, respectively. HSQ layers were etched for 200 seconds in a plasma mixture out of CF_4, HCF_3 and argon (recipe: pressure: 20.0 mT, ICP-RF: 300 ± 10 W, RIE-RF: 40 ± 10 W, Temp: 20 °C, sccm (CF_4): 5 cm^3 min^{-1}, sccm (HCF_3): 15 cm^3 min^{-1}, sccm (argon): 5 cm^3 min^{-1}). CYTOP and LCE layers were etched in dependence of the film thicknesses in oxygen plasma with a Trion Minilock III plasma etcher from Trion Technology (recipe: pressure: 20.0 mT, ICP-RF: 300 ± 10 W, RIE-RF: 20 ± 10 W, temperature: 20 °C, sccm (oxygen): 25 cm^3 min^{-1}). Remaining CYTOP and HSQ were either etched with the same recipes or removed by treating the samples in stirred hydrofluoroether Novec HFE-7300 over night at 50 °C.

Patterned LCE pieces were removed in water and placed on a microscope slide covered with 1000 or 10 000 cSt silicon oil. The temperature dependent actuation behaviour was analysed as described before.

Analysis of layer thicknesses, homogeneities and patterned LCE film structures

Film thicknesses and homogeneities (wavyness and roughness) as well as three-dimensional images of patterned LCEs were measured with profilometry based on white light confocal microscopy (profilometer model: NanoFocus® μsurf® from NanoFocus AG).

Two-dimensional images of patterned LCEs were measured and analysed with (polarised optical) microscopy (microscope model: Olympus BX51 from Olympus) and SEM (SEM model: Phenom™ from FEI Company™).

Conclusion

According to the process established in this work it is possible to structure stripes of oriented LCEs by a sequence of processing steps like spin-coating, illumination with light and etching (that is without steps like stretching and orientation in electric or magnetic fields) on a substrate. Thus LCEs can be processed like classical MEMS.

This got possible by using a perfluorinated photoresist with orthogonal solubility (processable from fluorinated solvents, not from organic solvents or water based systems), which does not cause LCE swelling during the processing steps (note: the LCE swells in organic solvents and its actuation depends on the director orientation, which is lost or strongly reduced during swelling and deswelling).

In addition, a photoalignment layer is used to orient the LCE. It allows a local selection of the director orientation by

patterning with linear polarised light. This enables – generally – to create variable director fields in the LCE, which are the precondition for more complex actuations of the microstructures accessible by structuring.[30]

Overall, it thus gets possible to prepare stripes of LCEs, with a resolution of 1.5–2.0 microns, which actuate through heating if their thickness is above a critical value (above 700 nm). Length variations (not bending) of 10 to 20% as well as bending were investigated. It is possible to generally integrate them into MEMS, if they stick on one side to the substrate.

While thicker unpatterned LCE films show only shrinkage or elongation (two-dimensional movement), the patterned stripes show – in addition – strong director dependent three-dimensional bending and twisting motions. Bending can be valuable for sophisticated MEMS devices where complicated motions are needed, while two-dimensional deformations can be used generally for movement processes in the plane.

The results encourage us to develop an automatic process to build a large amount of micro devices in a parallel procedure and to demonstrate the potential of LCEs in MEMS devices.

Conflicts of interest

There are no conflicts to declare.

Acknowledgements

RZ and HZ thank the DFG (Ze 230/26-1 and Za 276/20-1) for support of this work. CKO and WLC are grateful for support by the National Science Foundation (CHE-1709660). This work made use of Cornell NanoScale Facility, a member of the National Nanotechnology Coordinated Infrastructure (NNCI), which is supported by the National Science Foundation (Grant ECCS-1542081). Finally, we want to thank the ROLIC company for the gift of the photoalignment layer solution and Orthogonal Inc. for providing the photoresist set.

References

1 F. J. Davis, *J. Mater. Chem.*, 1993, **3**, 551.
2 J. Küpfer and H. Finkelmann, *Macromol. Rapid Commun.*, 1991, **12**, 717–726.
3 L. Liu, B. Geng, S. M. Sayed, B.-P. Lin, P. Keller, X.-Q. Zhang, Y. Sun and H. Yang, *Chem. Commun.*, 2017, **53**, 1844–1847.
4 C. Ohm, M. Brehmer and R. Zentel, *Adv. Mater.*, 2010, **22**, 3366–3387.
5 R. Zentel, G. F. Schmidt, J. Meyer and M. Benalia, *Liq. Cryst.*, 1987, **2**, 651–664.
6 P. Beyer, E. M. Terentjev and R. Zentel, *Macromol. Rapid Commun.*, 2007, **28**, 1485–1490.
7 E. K. Fleischmann and R. Zentel, *Angew. Chem., Int. Ed.*, 2013, **52**, 8810–8827.
8 T. Hessberger, L. Braun and R. Zentel, *Polymers*, 2016, **8**, 410.
9 T. Hessberger, L. B. Braun, F. Henrich, C. Müller, F. Gießelmann, C. Serra and R. Zentel, *J. Mater. Chem. C*, 2016, **4**, 8778–8786.
10 L. B. Braun, T. Hessberger and R. Zentel, *J. Mater. Chem. C*, 2016, **4**, 8670–8678.
11 S. Varghese, G. P. Crawford, C. W. M. Bastiaansen, D. K. G. De Boer and D. J. Broer, *Appl. Phys. Lett.*, 2005, **86**, 1–3.
12 S. K. Ahn, T. H. Ware, K. M. Lee, V. P. Tondiglia and T. J. White, *Adv. Funct. Mater.*, 2016, **26**, 5819–5826.
13 S. Varghese, S. Narayanankutty, C. W. M. Bastiaansen, G. P. Crawford and D. J. Broer, *Adv. Mater.*, 2004, **16**, 1600–1605.
14 M. E. McConney, A. Martinez, V. P. Tondiglia, K. M. Lee, D. Langley, I. I. Smalyukh and T. J. White, *Adv. Mater.*, 2013, **25**, 5880–5885.
15 C. Ohm, C. Serra and R. Zentel, *Adv. Mater.*, 2009, **21**, 4859–4862.
16 L. T. De Haan, J. M. N. Verjans, D. J. Broer, C. W. M. Bastiaansen and A. P. H. J. Schenning, *J. Am. Chem. Soc.*, 2014, **136**, 10585–10588.
17 L. T. De Haan, V. Gimenez-Pinto, A. Konya, T. S. Nguyen, J. M. N. Verjans, C. Sánchez-Somolinos, J. V. Selinger, R. L. B. Selinger, D. J. Broer and A. P. H. J. Schenning, *Adv. Funct. Mater.*, 2014, **24**, 1251–1258.
18 J. E. Stumpel, D. J. Broer and A. P. H. J. Schenning, *Chem. Commun.*, 2014, **50**, 15839–15848.
19 B. Klöckner, P. Daniel, M. Brehmer, W. Tremel and R. Zentel, *J. Mater. Chem. C*, 2017, **5**, 6688–6696.
20 L. B. Braun, T. G. Linder, T. Hessberger and R. Zentel, *Polymers*, 2016, **8**, 435.
21 A. H. Gelebart, M. Mc Bride, A. P. H. J. Schenning, C. N. Bowman and D. J. Broer, *Adv. Funct. Mater.*, 2016, **26**, 5322–5327.
22 C. L. van Oosten, C. W. M. Bastiaansen and D. J. Broer, *Nat. Mater.*, 2009, **8**, 677–682.
23 C. L. Van Oosten, D. Corbett, D. Davies, M. Warner, C. W. M. Bastiaansen and D. J. Broer, *Macromolecules*, 2008, **41**, 8592–8596.
24 H. P. C. Van Kuringen, Z. J. W. A. Leijten, A. H. Gelebart, D. J. Mulder, G. Portale, D. J. Broer and A. P. H. J. Schenning, *Macromolecules*, 2015, **48**, 4073–4080.
25 T. J. White and D. J. Broer, *Nat. Mater.*, 2015, **14**, 1087–1098.
26 T. Ikeda, J. I. Mamiya and Y. Yu, *Angew. Chem., Int. Ed.*, 2007, **46**, 506–528.
27 H. Yu and T. Ikeda, *Adv. Mater.*, 2011, **23**, 2149–2180.
28 H. Yang, G. Ye, X. Wang and P. Keller, *Soft Matter*, 2011, **7**, 815.
29 M. Wang, B.-P. Lin and H. Yang, *Nat. Commun.*, 2016, **7**, 13981.
30 S. Schuhladen, F. Preller, R. Rix, S. Petsch, R. Zentel and H. Zappe, *Adv. Mater.*, 2014, **26**, 7247–7251.
31 S. Petsch, R. Rix, B. Khatri, S. Schuhladen, P. Müller, R. Zentel and H. Zappe, *Sens. Actuators, A*, 2014, **231**, 44–51.
32 S. Petsch, B. Khatri, S. Schuhladen, L. Köbele, R. Rix, R. Zentel and H. Zappe, *Smart Mater. Struct.*, 2016, **25**, 85010.

33 E.-K. Fleischmann, H.-L. Liang, N. Kapernaum, F. Giesselmann, J. Lagerwall and R. Zentel, *Nat. Commun.*, 2012, **3**, 1178.
34 C. M. Waits, B. Morgan, M. Kastantin and R. Ghodssi, *Sens. Actuators, A*, 2005, **119**, 245–253.
35 Y. B. Jeon, R. Sood, J. H. Jeong and S. G. Kim, *Sens. Actuators, A*, 2005, **122**, 16–22.
36 H. Miyajima, *J. Microelectromech. Syst.*, 1995, **4**(4), 220–229.
37 R. Delille, M. G. Urdaneta, S. J. Moseley and E. Smela, *J. Microelectromech. Syst.*, 2006, **15**, 1108–1120.
38 S. V. Ahir, A. R. Tajbakhsh and E. M. Terentjev, *Adv. Funct. Mater.*, 2006, **16**, 556–560.
39 D. L. Thomsen, P. Keller, J. Naciri, R. Pink, H. Jeon, D. Shenoy and B. R. Ratna, *Macromolecules*, 2001, **34**, 5868–5875.
40 T. Mirfakhrai, J. D. W. Madden and R. H. Baughman, *Mater. Today*, 2007, **10**, 30–38.
41 A. Sánchez-Ferrer, T. Fischl, M. Stubenrauch, H. Wurmus, M. Hoffmann and H. Finkelmann, *Macromol. Chem. Phys.*, 2009, **210**, 1671–1677.
42 A. Sánchez-Ferrer, T. Fischl, M. Stubenrauch, A. Albrecht, H. Wurmus, M. Hoffmann and H. Finkelmann, *Adv. Mater.*, 2011, **23**, 4526–4530.
43 A. Sánchez-Ferrer, N. Torras, M. Duque, C. J. Camargo and J. Esteve, *Soft Matter*, 2017, **13**, 7264–7272.
44 A. S.-F. Núria Torras, K. E. Zinoviev and J. Esteve, *J. Mater. Chem. C*, 2013, **1**, 5183–5190.
45 D. Liu and D. J. Broer, *Langmuir*, 2014, **30**, 13499–13509.
46 B. A. Kowalski, V. P. Tondiglia, T. Guin and T. J. White, *Soft Matter*, 2017, **13**(24), 4335–4340.
47 M. P. Van, C. W. M. Bastiaansen and D. J. Broer, *Adv. Opt. Mater.*, 2016, **4**, 677–681.
48 M. Bründel, M. Stubenrauch, H. Wurmus and A. Sánchez-ferrer, *International Newsletter on Micro-Nano Integration (MST-NEWS)*, 2004, vol. **4**, pp. 38–39.
49 K. Nickmans, J. N. Murphy, B. de Waal, P. Leclère, J. Doise, R. Gronheid, D. J. Broer and A. P. H. J. Schenning, *Adv. Mater.*, 2016, **28**, 10068–10072.
50 M. H. L. A. Buguin, P. Silberzan, B. Ladoux and P. Keller, *J. Am. Chem. Soc.*, 2006, **128**, 1088.
51 A. Sánchez-Ferrer, N. Torras and J. Esteve, Integration of Liquid-Crystalline Elastomers in MEMS/MOEMS, in *Liquid Crystalline Polymers: Volume 1-Structure and Chemistry*, ed. V. Thakur, M. Kessler, Springer Cham., 2016, ch. 19, pp. 553–582.
52 J. K. Lee, M. Chatzichristidi, A. A. Zakhidov, P. G. Taylor, J. A. DeFranco, S. H. Ha, H. F. Hon, A. B. Holmes, G. G. Malliaras and C. K. Ober, *J. Am. Chem. Soc.*, 2008, **130**, 11564–11565.
53 P. G. Taylor, J. K. Lee, A. A. Zakhidov, M. Chatzichristidi, H. H. Fong, J. A. DeFranco, G. G. Malliaras and C. K. Ober, *Adv. Mater.*, 2009, **21**, 2314–2317.
54 A. A. Zakhidov, J.-K. Lee, J. A. DeFranco, H. H. Fong, P. G. Taylor, M. Chatzichristidi, C. K. Ober and G. G. Malliaras, *Chem. Sci.*, 2011, **2**, 1178.
55 A. A. Zakhidov, J. K. Lee, H. H. Fong, J. A. DeFranco, M. Chatzichristidi, P. G. Taylor, C. K. Ober and G. G. Malliaras, *Adv. Mater.*, 2008, **20**, 3481–3484.
56 V. Linder, B. D. Gates, D. Ryan, B. A. Parviz and G. M. Whitesides, *Small*, 2005, **1**, 730–736.
57 J. Schmidtke, S. Kniesel and H. Finkelmann, *Macromolecules*, 2005, **38**, 1357–1363.
58 A. Komp, J. Rühe and H. Finkelmann, *Macromol. Rapid Commun.*, 2005, **26**, 813–818.
59 M. Ibn-Elhaj, S. Chappellet and F. Lincker, *Solid State Phenom.*, 2011, **181–182**, 3–13.
60 C. Ohm, E. K. Fleischmann, I. Kraus, C. Serra and R. Zentel, *Adv. Funct. Mater.*, 2010, **20**, 4314–4322.
61 L. A. Pederson, *J. Electrochem. Soc.*, 1982, **129**(1), 205–208.
62 J. L. Grant, D. S. Dunn and D. J. McClure, *J. Vac. Sci. Technol., A*, 1988, **6**, 2213.
63 S. J. Moss, *Polym. Degrad. Stab.*, 1987, **17**, 205–222.
64 G. N. Taylor and T. M. Wolf, *Polym. Eng. Sci.*, 1980, **20**, 1087–1092.
65 A. Vesel and T. Semenič, *Mater. Tehnol.*, 2012, **46**, 227–231.
66 W. L. Chen, M. Menzel, T. Watanabe, O. Prucker, J. Rühe and C. K. Ober, *Langmuir*, 2017, **33**, 3296–3303.
67 W. L. Chen, M. Menzel, O. Prucker, E. Wang, C. K. Ober and J. Rühe, *Macromolecules*, 2017, **50**, 4715–4724.
68 A. Pimpin and W. Srituravanich, *Eng. J.*, 2012, **16**, 37–55.
69 H. Zeng, O. M. Wani, P. Wasylczyk, R. Kaczmarek and A. Priimagi, *Adv. Mater.*, 2017, **29**, 1–7.

